Mercury's Exosphere during MESSENGER's Second Flyby: Detection of Magnesium and Distinct Distributions of Neutral Species

William E. McClintock[1*], Ronald J. Vervack, Jr.[2], E. Todd Bradley[3], Rosemary M. Killen[4], Nelly Mouawad[4], Ann L. Sprague[5], Matthew H. Burger[4], Sean C. Solomon[6], and Noam R. Izenberg[2]

[1]Laboratory for Atmospheric and Space Physics, University of Colorado, Boulder, CO 80303, USA. [2]The Johns Hopkins University Applied Physics Laboratory, Laurel, MD 20723, USA. [3]Department of Physics, University of Central Florida, Orlando, FL 32816, USA. [4]Department of Astronomy, University of Maryland, College Park, MD 20742, USA. [5]Lunar and Planetary Laboratory, The University of Arizona, Tucson, AZ 85721, USA. [6]Department of Terrestrial Magnetism, Carnegie Institution of Washington, Washington, DC 20015, USA.

*To whom correspondence should be addressed. E-mail: william.mcclintock@colorado.edu Telephone: (303) 492-8407, Fax: (303) 492-6444

Observations of Mercury's exosphere during MESSENGER's second flyby on 6 October 2008 detect magnesium and show differences among the distributions of neutral sodium, calcium, and magnesium.

Submitted to *Science* 18 February 2009

During MESSENGER's second Mercury flyby, the Mercury Atmospheric and Surface Composition Spectrometer observed emission from Mercury's neutral exosphere. These observations include the first detection of emission from magnesium. Differing spatial distributions for sodium, calcium, and magnesium were revealed by observations beginning in Mercury's tail region, approximately 8 Mercury radii anti-sunward of the planet, continuing past the nightside, and ending near the dawn terminator. Analysis of these observations, supplemented by observations during the first Mercury flyby as well as those by other MESSENGER instruments, suggests that the distinct spatial distributions arise from a combination of differences in source, transfer, and loss processes.

While the interface between the planetary surface and external space environment is a classical, collision-dominated atmosphere for the three largest terrestrial planets, Mercury's interface is a tenuous, surface-bounded exosphere in which the constituent atoms and molecules travel on collisionless trajectories and are far more likely to impact the surface than to interact with each other. Mercury's exospheric properties are primarily determined by the interaction of the surface with the space environment. The planet's highly elliptical orbit and proximity to the Sun lead to strong seasonal variations in exospheric density distributions (*1, 2*). In addition, Mercury's intrinsic magnetic field interacts with the interplanetary medium to modulate the spatial distribution and density of solar wind plasma and high-energy charged particles that reach the planet's surface and sputter materials from it. This interaction leads to changes in exospheric

densities that vary on timescales as short as a few hours *(3)*. Impacts also supply both meteoritic and volatilized surface materials to the exosphere.

Species that have been detected in Mercury's exosphere include hydrogen (H) and helium (He), which were measured by the Mariner 10 Ultraviolet Spectrometer (*4, 5*), and sodium (Na), potassium (K), and calcium (Ca), which were discovered with ground-based telescopes (*6–8*). Neutral species released from the surface with sufficient energy are accelerated by solar radiation pressure to form an extended, anti-sunward tail of neutral atoms, as demonstrated by ground-based observations of Mercury's Na tail (*9–11*). Here we report observations of Mg, Ca, and Na in Mercury's exosphere and tail obtained with the Ultraviolet and Visible Spectrometer (UVVS) channel of the Mercury Atmospheric and Surface Composition Spectrometer (MASCS) (*12*) made on 6 October 2008 during the second Mercury flyby by the MErcury Surface, Space ENvironment, GEochemistry, and Ranging (MESSENGER) spacecraft (*13*).

Observations made by the UVVS during the first Mercury flyby on 14 January 2008 revealed a distinct north-south asymmetry (25% brighter in the north) to the sodium (Na) tail and a near-planet, nightside calcium (Ca) distribution with a strong dawn-dusk asymmetry (10 times brighter toward the dawn) (*14*). To explore these structures further, observations during the second flyby included simultaneous measurements of both of these species as well as neutral magnesium (Mg), beginning in Mercury's tail approximately 8 R_M (R_M is Mercury's radius, 2440 km) anti-sunward of the planet, continuing through the nightside, near-planet exosphere, and ending near the dawn terminator. The observations were restricted to narrow wavelength ranges centered on the resonant emission lines of the species at 285.2 nm (Mg), 422.7 nm (Ca), and 589.0 and 589.6 nm (Na D2 and D1 lines). These observations confirmed the persistence of Na and Ca structures seen in the first flyby. In addition, they resulted in the first detection of neutral

Mg in Mercury's exosphere. Simultaneous measurements of these three species along nearly identical, narrow lines of sight allow their spatial distributions to be compared and contrasted in order to constrain individual source, transport, and loss processes for each.

Observations of the D lines of Na began in the tail region approximately 56,000 km (23 R_M) behind the planet. At approximately 35,000 km from the planet the UVVS switched observing programs to include the Mg and Ca resonance lines. This observing program continued until the spacecraft was approximately 5000 km from the planet. Although the Na was clearly present from the beginning, the Ca and Mg emissions were detected with statistical significance only at distances less than 19,500 km (8 R_M).

During the tail observations the spacecraft rolled up and down about the Sun-Mercury line, scanning the UVVS 0.1° × 1.0° field of view across a plane defined by the Sun-Mercury line and Mercury's north pole. As the spacecraft rotated, spectra from Mg, Ca, and Na were recorded in rapid succession along nearly identical lines of sight. The observations were designed to sweep the line-of-sight intercept with the plane through a vertical distance bounded by ±3 R_M. This objective required the rotation angle to increase monotonically from ±5° to ±40° as the spacecraft approached the planet [see Fig. 1A in (*14*)]. Therefore, the UVVS viewed a larger angular region of space as the tail observations progressed. In addition, the line of sight often crossed Mercury's shadow, complicating density determinations because the observed resonance lines are excited by solar illumination, and atoms in the shadow region do not emit. The relative strength of the emission as a function of look direction, however, is a robust measurement because the UVVS effectively integrates from the spacecraft to infinity.

Figure 1 displays sums of 100 spectra obtained from each species over the range 8 R_M to 2 R_M. Each spectrum consists of either 16 wavelength steps (Mg and Ca) or 18 wavelength steps

(Na D lines) and includes the emission line plus detector dark counts (5 steps centered on the emitting wavelength) as well as the detector dark counts on either side. Figure 1 also compares the emission from Mg, Ca, and Na in the tail region. Here detected photon counts have been converted to column emission, expressed in Rayleighs (1 R=10^6 photons cm^{-2} s^{-1} emitted into 4π steradians), using instrument calibration coefficients, determined during ground tests (*12*). These column emissions were projected onto the Sun–Mercury/north-pole plane to produce a two-dimensional representation of the distributions. While the Na emission exhibits a distinct high-latitude enhancement relative to the equatorial regions, Ca emission peaks near the equatorial regions and declines toward higher latitudes. The Mg emission appears to be nearly uniformly distributed but shows evidence for a weak, double-lobed, north-south enhancement. Signals from both Mg and Ca are weaker than for Na; therefore, some of the variations seen in Figure 1 result from detector count noise, which, after conversion to radiance, have 1-standard-deviation values of 11, 9, and 75 R for Mg, Ca, and Na, respectively.

Figure 1 also compares the latest Na tail observations to those from the first MESSENGER flyby (*14*). Although slight viewing geometry differences do not allow for a direct comparison of the two, both flybys show an enhancement of emission at higher latitudes, a pattern noted in ground-based observations (*10*) and ascribed to variations in the solar-wind-sputtering source component of Na atoms. Flybys 1 and 2 occurred at Mercury true anomaly 285.3° and 293.6°, respectively, so that differences in the exosphere resulting from seasonal variations are expected to be small.

Once the spacecraft entered Mercury's shadow, the UVVS carried out a "fantail" series of observations to explore the near-planet exosphere (Figs. 2A and 2C). These began with the UVVS line of sight pointed in Mercury's equatorial plane toward the dawn hemisphere. They

continued as the spacecraft executed a 180° roll through north, and finished with the line of sight pointed near the equatorial plane toward the dusk hemisphere. Immediately following the fantail, the UVVS line of sight intersected the nightside surface of the planet. As the spacecraft passed through closest approach and began its outbound leg, it emerged from Mercury's shadow. Although the line of sight still intersected the nightside surface, at least some part of the column between the spacecraft and surface was illuminated and resulted in measurable emission (Figs. 2B and 2D). These observations continued until the line of sight crossed the dawn terminator, at which point sunlight reflected from the bright dayside disk precluded exospheric observations.

As with the tail observations, both the fantail and near-terminator observations showed differing spatial distributions of the three species. Ca emission peaked near the dawn equator and monotonically declined during the rotation to the dusk direction. Na emission was weakest in the dawn direction, passed through a maximum near the north pole, and declined slightly toward dusk. In contrast, Mg emission remained more or less uniform throughout the fantail. During the near-terminator observations, all three species showed an increase in emission intensity as the illuminated column along the line of sight increased in length while the spacecraft approached the dayside. While the Ca and Mg emissions grew at a rate proportional to the illuminated column length, Na emission increased more rapidly.

Observations of the dayside exosphere close to the planet concentrated on hydrogen (H). The measured distribution is consistent with the "warm" component of H observed by Mariner 10 (*4*) and during the first MESSENGER flyby (*14*). These data are not discussed further here.

The principal processes that liberate material from the surface and populate the exosphere include thermal desorption, photon-stimulated desorption, electron-stimulated desorption, meteoroid-impact vaporization, and ion sputtering (e.g., *15*). Ion sputtering followed by

meteoroid-impact vaporization are the most energetic; and these processes, acting on regions of the surface near the terminator, likely provide the bulk of material observed in the tail region. Once species are lofted above the surface, their distributions are determined by gravity, radiation pressure, and photoionization followed by magnetic and electric field transport ending in either a rapid loss to the system along open lines or a return to the surface. The relevant transport and ionization lifetimes (*16, 17)* vary greatly for Mg, Ca, and Na (Table 1).

During flyby 2, the north-south sweeps exhibited no detectable modulation of Na in the far tail, but rather a uniform brightness of 610 R at 56,000 km that increased as the inverse square of the distance from planet center. Near 22,000 km, where flyby 2 measurements first overlap those from flyby 1, radiance values of 3,640 R (flyby 2) and 3,420 R (flyby 1) were nearly identical, and the flux of Na escaping down the tail was $\sim 6 \times 10^{23}$ atoms s^{-1} at both encounters. That neutral Na can reach great distances is a consequence of its relatively long lifetime coupled with intense radiation pressure. Atoms released from the surface with antisunward velocities as small as 1.4 km s^{-1}, corresponding to 0.23 electron volts (eV) of kinetic energy, are accelerated down the tail approximately 35 R_M, to a velocity of 8 km s^{-1}, in one ionization lifetime.

Closer to the planet, the Na tail emissions observed during both MESSENGER flybys display distributions peaked at high latitudes (Figs. 1F and 1G), a feature commonly seen in ground-based observations (*10, 18–20*). These enhancements are consistent with a scenario in which energetic Na ions are ejected from the surface by ion sputtering at high latitudes (*10, 19*). The conclusion that there is significant north-south enhancement is robust, although tracings of the lines of sight through a detailed, three-dimensional model are required to rule out the possibility that some fraction results from an observational bias produced by the larger out-of-plane viewing angles that occur near the end of the tail observations. A north-south enhancement is further

supported by the fantail observations of Na, which also showed a significant north polar enhancement (Figs. 2A and 2C). If the Na distribution were symmetric about the Sun-Mercury line, the fantail would show uniformly increasing emission as the line of sight rolled from dawn to dusk because the field of view would intersect a monotonically increasing density (and therefore monotonically increasing emission brightness) while the spacecraft approached the planet's nightside. The ratio of observed emission in the dawn and dusk directions is compatible with a distribution that is symmetric about the Sun-Mercury line and increases toward the terminator, as would result from a symmetric source process such as photon-stimulated desorption; however, the northern excess requires an additional, high-latitude source of Na atoms, most probably related to solar-wind sputtering of Na atoms (see Fig. 2C).

During the first flyby, Na emission appeared relatively bright in the northern hemisphere [Fig. 1G; see also Fig. 1 (*14*)]. This was in contrast with nearly uniform north-south emission strength observed in the second flyby. This result is consistent with MESSENGER magnetosphere observations, which suggest that the solar wind plasma impingement on Mercury's surface was directed toward higher northern latitudes during the first flyby but more uniformly distributed during the second flyby (*21–24*).

In contrast to Na, the UVVS Ca tail observations show a definite equatorial peak and no high-latitude enhancements (Fig. 1E), indicating that Ca is not uniformly distributed about the planet. This conclusion is further supported by the clear concentration of Ca emission in the dawn equatorial region during the fantail observations (Figs. 2A and 2C). Calcium's ionization lifetime at Mercury is 1,700 s, and the effect of radiation pressure is relatively small; therefore, Ca atoms released from the surface must be extremely energetic (~ 5-7 eV) in order to travel down the tail to 4 or 5 Mercury radii before being ionized. If Ca atoms were released to the

exosphere by solar-wind sputtering or by meteoroid impact, this result would imply that the observed Ca comes from the high-energy tail of the source process and could explain why Ca in the exosphere appears to be depleted by two orders of magnitude relative to Na (*8*). Alternatively, it has been suggested that Ca is released as CaO and may be rapidly expanding after dissociation from a parent molecule that was earlier released into the exosphere (e.g., *25*). The dawn-dusk asymmetry in Ca emission, observed in both flybys, could have a contribution from enhanced meteoroid impact velocity and flux on the dawn side resulting from Mercury's orbital motion.

Absorption by the Earth's atmosphere prohibits ground-based observation of the Mg 285.2 nm resonance line; and the UVVS observations provide the first detection of the Mg distribution about Mercury. Although the Mg tail (Fig. 1C) and fantail emissions (Figs. 2A and 2C) are most consistent with an isotropic distribution, there is statistically significant evidence for weak high-latitude components in the tail. Although Mg and Ca are chemically similar, the atomic mass of Mg is a factor of 1.65 smaller than Ca and its ionization lifetime 124 times longer. Radiation pressure is negligible for Mg, so that an antisunward release velocity of 3.7 km s^{-1}, corresponding to ~ 1.7 eV minimum (> 2.4 eV average) energy, is required to propel it to an altitude of ~ 4 R_M; and a radial velocity of 4.3 km s^{-1} is required for escape. The small radiation pressure and long lifetime suggests that the majority of the Mg atoms will most likely return to the surface rather than be photoionized like Ca or escape down the tail like Na.

In the near-terminator region, the observed emissions from the exosphere increase as the illuminated column between the spacecraft and the surface grows. Line plots of emission as functions of line-of-sight distance behind the terminator (Fig. 2D) reveal a more rapid increase

for Na than for Ca and Mg. This difference is consistent with the view that there is a significant concentration of low-energy Na relative to Ca and Mg near the terminators.

In the fantail and near-terminator regions, emission rates were converted to approximate line-of-sight abundances using column density factors (Table 1) calculated from g-values (the emission probability per atom, expressed as photons s^{-1} $atom^{-1}$) for atoms at rest with respect to Mercury (*26*). These estimates indicate that while the Na and Mg abundances in the near-planet exosphere are comparable, those for Ca are smaller by a factor of ~50–100. It is possible that the relative amounts of Mg, Ca, and Na released from the surface are comparable and the difference results from the relatively short Ca lifetime; alternatively, it could indicate that the abundance of Ca in the surface materials is less than that of Mg and Na.

Analysis of global-scale color images obtained during the MESSENGER flybys points to a significant Mg component in Mercury's crust (*27*) and ground-based spectroscopic observations of Mercury's regolith indicate the presence of Mg-bearing minerals as well as those of Ca and Na (*28*). The observed exospheric Mg, Ca, and Na derive from these surface minerals as well as from implanted solar wind atoms and meteoroids that impact the planet. Synoptic observations can provide the data to disentangle the relative contributions of these sources.

References and Notes

1. W. H. Smyth, M. L. Marconi, *Astrophys. J.*, **441**, 839 (1995).
2. A. E. Potter, R. M. Killen, T. H. Morgan, *Icarus* **186**, 571 (2007).
3. R. M. Killen, M. Sarantos, A. E. Potter, P. Reiff, *Icarus* **171**, 1 (2004).
4. A. L. Broadfoot, S. Kumar, M. J. S. Belton, M. B. McElroy, *Science* **185**, 166 (1974).
5. D. E. Shemansky, A. L. Broadfoot, *Rev. Geophys. Space Phys.* **15**, 491 (1977).
6. A. E. Potter, T. H. Morgan, *Science* **229**, 651 (1985).

7. A. E. Potter, T. H. Morgan, *Icarus* **67**, 336 (1986).

8. T. Bida, R. M. Killen, T. H. Morgan, *Nature* **404**, 159 (2000).

9. A. E. Potter, R. M. Killen, T. H. Morgan, *Meteorit. Planet. Sci.* **37**, 1165 (2002).

10. A. E. Potter, R. M. Killen, *Icarus* **194**, 1 (2008).

11. J. Baumgardner, J. Wilson, M. Mendillo, *Geophys. Res. Lett.* **35**, L03201, 10.1029/2007GL032337 (2008).

12. W. E. McClintock, M. R. Lankton, *Space Sci. Rev.* **131**, 481 (2007).

13. S. C. Solomon *et al.*, *Space Sci. Rev.* **131**, 3 (2007).

14. W. E. McClintock *et al.*, *Science* **321**, 90 (2008).

15. R. M. Killen *et al.*, *Space Sci. Rev.* **132**, 433 (2007).

16. W. F. Huebner, J. J. Keady, S. P. Lyon, *Astrophys. Space Sci.* **195**, 1 (1992).

17. W. F. Huebner, private communication (2009).

18. A. L. Sprague *et al.*, *Icarus* **129**, 506 (1997).

19. R. M. Killen *et al.*, *J. Geophys. Res.*, **106**, 20509 (2001).

20. F. Leblanc *et al.*, *Geophys. Res. Lett.* **35**, L18204, 10.1029/2008GL035322 (2008).

21. J. A. Slavin *et al.*, *Science* **321**, 85 (2008).

22. B. J. Anderson *et al.*, *Eos Trans. AGU* **89***(53)*, Fall Meet. suppl., U12A-04 (2008).

23. J. A. Slavin *et al.*, *Science,* this issue (2009).

24. M. Sarantos *et al.*, *Geophys. Res. Lett.* **36**, 10.1029/2008GL036207 (2009).

25. R. M. Killen, T. A. Bida, T. H. Morgan, *Icarus* **173**, 300 (2005).

26. R. M. Killen, D. E. Shemansky, N. Mouawad, *Astrophys. J. Suppl.,* in press (2009).

27. B. W. Denevi *et al.*, *Science,* this issue (2009).

28. A. L. Sprague *et al.*, *Planet. Space Sci.*, in press (2009).

29. We thank Walter F. Huebner for providing us with unpublished ionization rates for Mg and Ca. Mark Lankton and Mark Kochte made important contributions to the acquisition and analysis of the data reported here. The MESSENGER project is supported by the NASA Discovery Program under contracts NAS5-97271 to The Johns Hopkins University Applied Physics Laboratory and NASW-00002 to the Carnegie Institution of Washington. RJV, RMK, and ALS are supported by the MESSENGER Participating Scientist Program.

Table 1. Transport and photoionization parameters

Species	Radiation acceleration/ surface gravity*	Ionization lifetime (s)	Column density factor* (atoms $cm^{-2} R^{-1}$)
Mg	4.7×10^{-3}	2.1×10^{5}	3.15×10^{6}
Ca	0.12	1.7×10^{3}	4.42×10^{4}
Na	0.47	2.0×10^{4}	1.63×10^{4}

*Acceleration due to radiation pressure as a fraction of surface gravity and column density factor for an atom at rest with respect to Mercury (-9.5 km s^{-1} with respect to the Sun) at the true anomaly angle corresponding to the time of the second MESSENGER flyby. As Na and Ca atoms accelerate antisunward, the presence of deep absorption lines in the solar spectrum causes first a decrease in these values followed by an increase.

Figure 1

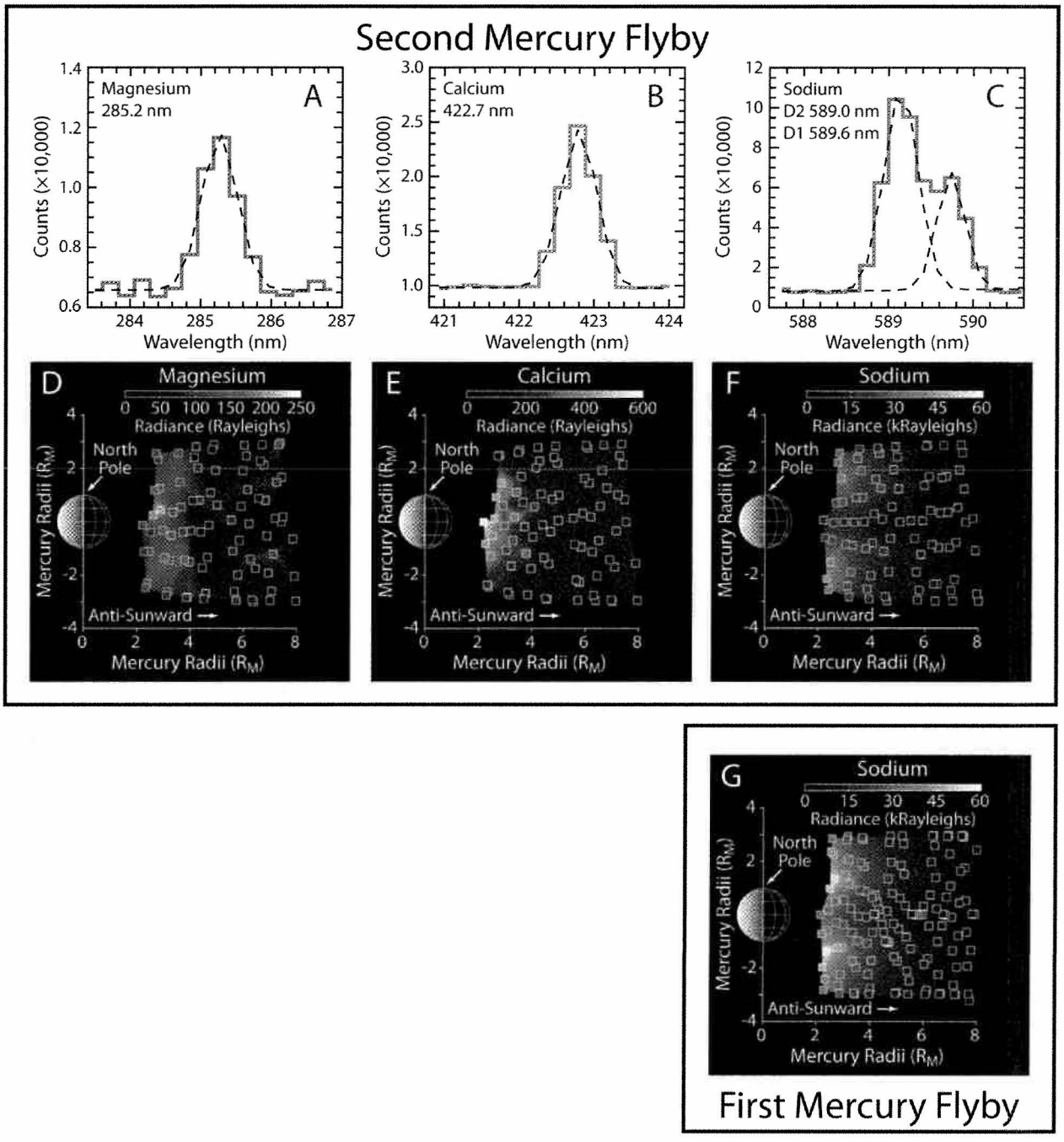
Second Mercury Flyby
Magnesium
285.2 nm
A
Calcium
422.7 nm
B
Sodium
D2 589.0 nm
D1 589.6 nm
C
Counts (×10,000)
Wavelength (nm)
D
Magnesium
Radiance (Rayleighs)
E
Calcium
Radiance (Rayleighs)
F
Sodium
Radiance (kRayleighs)
North Pole
Anti-Sunward
Mercury Radii (R_M)
G
Sodium
Radiance (kRayleighs)
First Mercury Flyby

Fig. 1. Example emission spectra and radiance maps from the tail observations. (**A-C**) Sums of 100 spectra obtained for each species over the distance range 8 R_M to 2 R_M. These spectra have been fit with Gaussian functions (dashed lines) in order to delineate the emission profile. The UVVS detectors are photon-counting photomultiplier tubes. Their signals are total numbers of photon counts, and each uncertainty is the square root of the total number of counts (photons plus dark). Thus, the measured signal-to-noise ratios are 119, 204, and 679, for Mg, Ca, and Na, respectively. (**D-F**) Emission from Mg, Ca, and Na during the tail observations described in the text. Individual observations (white squares) are overlaid on an image generated by projecting the observed line-of-sight emissions onto a plane containing the Sun-Mercury line and the planet's north pole and interpolating to fill in regions not observed. (**G**) The Na tail emission from the first Mercury flyby, truncated at 2.1 R_M anti-sunward to match the spatial coverage obtained here, is shown for comparison.

Figure 2.

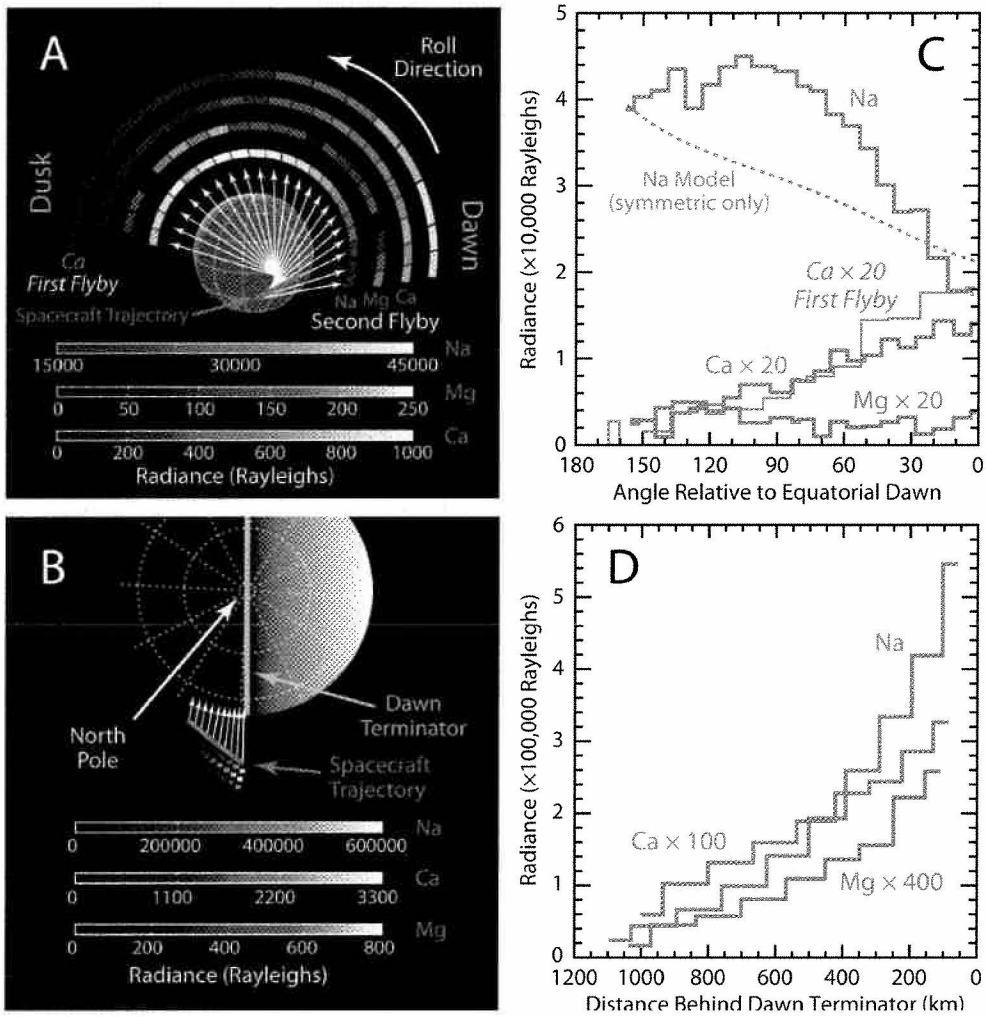
A
Roll Direction
Dusk
Dawn
Ca First Flyby
Spacecraft Trajectory
Na Mg Ca
Second Flyby
Na
15000 30000 45000
Mg
0 50 100 150 200 250
Ca
0 200 400 600 800 1000
Radiance (Rayleighs)
B
North Pole
Dawn Terminator
Spacecraft Trajectory
Na
0 200000 400000 600000
Ca
0 1100 2200 3300
Mg
0 200 400 600 800
Radiance (Rayleighs)
C
Na
Na Model (symmetric only)
Ca × 20 First Flyby
Ca × 20
Mg × 20
Radiance (×10,000 Rayleighs)
0 1 2 3 4 5
180 150 120 90 60 30 0
Angle Relative to Equatorial Dawn
D
Na
Ca × 100
Mg × 400
Radiance (×100,000 Rayleighs)
0 1 2 3 4 5 6
1200 1000 800 600 400 200 0
Distance Behind Dawn Terminator (km)

Fig. 2. Emission from Na, Ca, and Mg during (**A**) the "fantail" and (**B**) the near-dawn-terminator. The arrows in each panel indicate the direction of the UVVS line of sight during the Na observations. During the fantail, the line of sight rotated 180° from viewing the equatorial dawn hemisphere region through north to finish viewing the equatorial dusk hemisphere. During the near-terminator observations, the line of sight is pointed at the surface of Mercury, approximately in the equatorial plane. In both images, the lines of sight for Ca and Mg are approximately equally spaced between adjacent Na observations because the three species are measured consecutively before the sequence repeats. (**C**) Line plots of the fantail emissions show a steep increase in Na emission as the line of sight rotates toward north followed by a gentle decline toward dusk. A model profile consistent with emission from a Na distribution that increases toward the terminator and is symmetric about the Sun-Mercury line (dashed line; calculated from a model that includes symmetric impact vaporization and photon-stimulated desorption sources only) must be supplemented by an additional component concentrated to the north to reproduce the observations. In contrast, Ca exhibits a nearly linear decline from dawn to dusk, consistent with being most abundant toward dawn, while Mg is approximately uniform with direction. Ca emission observed in similar sequences during the first Mercury flyby (thin green line) showed nearly identical fantail behavior. In the near-terminator region the observed emissions from the exosphere increase as the illuminated column length between the spacecraft and the surface grows. (**D**) Line plots of emission as functions of line-of-sight distance behind the terminator reveal a more rapid increase for Na than for Ca and Mg.